Optical Properties of Self-Assembled 2D and 3D Superlattices of Silver Nanoparticles

A. Taleb,[†] C. Petit,[†,‡] and M. P. Pileni*[,†,‡]

Laboratoire SRSI, URACNRS 1662, Université P. et M. Curie (Paris VI), BP 52, 4 Place Jussieu, F-752 31 Paris Cedex 05, France, and CEA-Saclay, DRECAM-SCM, F-911 91 Gif-sur-Yvette, Cedex, France

Received: August 25, 1997; In Final Form: December 2, 1997

In this paper we compare the optical properties of nanosized silver particles dispersed in hexane solution and self-assembled in a 2D or 3D network. When the particles form monolayers organized in a hexagonal network, the plasmon peak of silver nanosized particles is shifted toward lower energy, with an increase in bandwidth compared to that observed with free coated particles dispersed in hexane solution. Such a shift is attributed to an increase in the dielectric constant of the matrix environment of the nanoparticles. When the particles form a 3D superlattice with a face-centered cubic (fcc) structure, the optical properties could be interpreted as an increase in the mean free path of the conduction electrons, which could indicate the presence of tunneling electrons across the double layers due to the coating of the particles.

I. Introduction

The engineering of materials and devices on the nanoscale is of great current interest in electronics and optics than is the engineering of either isolated molecules or macroscopic solids. Confinement and quantization of conduction electrons within a small volume[1−3] enhance the optical and electronic conductance properties of materials composed of nanocrystals. In the past two decades the unusual size-dependent electronic properties of small metal particles have motivated a vast amount of work concerned with the simulated optical properties, preparation, and characterization of a wide range of new clusters.[4,5−10]

Well-defined, ordered solids prepared from tailored nanocrystallites building blocks provide opportunities for optimizing properties of materials and offer possibilities for observing interesting, new, and potentially useful collective physical phenomena. In the past few years, several techniques have been developed for directing the self-assembly of nanocrystals into ordered aggregates or quantum dots superlattices.[11−21] These assemblies present some very exciting possibilities. In principle, interparticle separations, particle size, and particle stoichiometry may be individually manipulated to produce a macroscopic solid. This is similar to the well-known case of a one-dimensional quantum dot superlattice which might be engineered to exhibit unique physical properties. Such materials could be important constituents of tunnel resonance resistors[22] in novel microelectronic devices.

Large classes of material can be produced by using reverse micelles as templates.[11,12] Several years ago, by using this technique, we demonstrated that nanosized silver metal particles can be produced with control of the particle size from 2 to 8 nm.[23] The optical properties of these clusters confirm simulation-based predictions. To decrease the size distribution, a size selection precipitation method was used.[24] Particles were arranged either in monolayers organized in a hexagonal network or in 3D superlattices with a face-centered cubic (fcc) structure.[24] Similar arrangements were obtained few years ago with silver sulfide nanoparticles.[25−27] By using different preparation modes, several groups succeed to form similar patterns with gold and silver nanosized particles.[28−32]

In the present paper, we compare the optical properties of silver nanosized particles dispersed in a solvent and arranged in 2D and 3D superlattices.

II. Experimental Section

1. Products. AOT was purchased from Sigma. Isooctane, hexane, and pyridine were purchased from Fluka. Hydrazine and dodecanethiol were obtained from Prolabo (France) and Janssen Chemicals, respectively. The materials were not purified any further.

Silver bis(2-ethylhexyl)sulfosuccinate, Ag(AOT), has been prepared as described previously.[33]

2. Apparatus. Absorption spectra were recorded on a conventional Varian Cary 1 spectrophotometer (in 1- or 2-mm cuvettes). The Cary 1/3 internal diffuse reflectance accessory is used for 2D or 3D film absorption.

The transmission electron microscope (JEOL 100CX) operates at 100 kV. The mean diameter, D_m, and the standard deviation, σ_m, were derived from an average number of 500 particles. The polydispersity is defined as the ratio σ_m/D_m.

Scanning electron microscopy, SEM, is performed with a JEOL JSM840 A microscope.

III. Optical Properties of Colloidal Silver Particles

Optical properties of isolated colloidal particles and, in particular, their dependence on size effect[34−36,47] have been intensively investigated. Absorption spectra of metal colloidal dispersions exhibit broad bands in the UV−visible range due to the excitation of plasma resonances or interband transitions. The UV−visible absorption spectra of a fairly dilute dispersion of colloidal particles can be calculated from the "Mie" theory.[4] The absorbance, A, for a dispersion of N particles per unit volume is given by[37]

$$A = CNl/2.303 \quad (1)$$

* To whom all correspondence should be addressed.
[†] Laboratoire SRSI, URACNRS 1662.
[‡] CEA-Saclay, DRECAM-SCM.

S1089-5647(97)02807-1 CCC: $15.00
Published on Web 03/03/1998

where C and l are the absorption cross section and the optical path length, respectively.

If the particle dimensions are smaller than the mean free path of the conduction electrons, collisions of these electrons with the particle surface take place. This lowers the effective mean free path. In the limit of $2\pi R < \lambda$ (where R is the radius of the particles and λ the wavelength of light in the media), only the electric dipole term, developed in Mie's theory, is significant. Then the cross section can be expressed as

$$C = (18\pi V\epsilon_2(\omega)\epsilon_m^{3/2})/\lambda[(\epsilon_1(\omega) + 2\epsilon_m)^2 + \epsilon_2(\omega)^2] \quad (2)$$

where V and λ are, respectively, the volume of the spherical particle and the incident wavelength, corresponding to a frequency ω. The complex relative permittivity of the metal, $\epsilon(\omega)$, is expressed as

$$\epsilon(\omega) = \epsilon_1(\omega) + i\epsilon_2(\omega)$$

When ϵ_2 is small or does not change so much around the band, the position of maximum absorption occurs for all $\epsilon_1(\omega) = -2\epsilon_m$. The wavelength of this plasma resonance is therefore given by the wavelength dependence of $\epsilon_1(\omega)$. The width and height of the resonance are determined by the $\epsilon_2(\omega)$ value at this wavelength. Furthermore, the plasmon peak width is related to the dielectric constant of the surrounding environment, ϵ_m.[36,38,39]

If the particle sizes are comparable to the mean free path of the conduction electrons, the collisions of conduction electrons with the particle surfaces become appreciable and thus the effective mean free path is less than that in bulk material. The electron energy bands are quantized and the number of discrete energy levels is related to the magnitude of the number of atoms in the crystal. For particles containing only 100 atoms, the intensities between the conduction band levels of metal particles are no longer smeared out thermally. This influences intraband transitions of the conduction electrons and leads to a damping of electron motion, which corresponds to the free path effect in the classical approach. This damping affects the dielectric constant.

To take into account the interband contribution and the size effect, it is necessary to split the dielectric function in two terms:[7,40] the first one, indexed IB, accounting for the 4d electron, and the second one, indexed F, considering the size effects due to the confinement of the free electron in small particles:

$$\epsilon_1(\omega) = \epsilon_{1IB}(\omega) + \epsilon_{1F}(\omega)$$

and

$$\epsilon_2(\omega) = \epsilon_{2IB}(\omega) + \epsilon_{2F}(\omega) \quad (3)$$

where

$$\epsilon_{1F}(\omega) = 1 - \{\omega_p^2/(\omega^2 + \omega_0^2)\}$$

and

$$\epsilon_{2F}(\omega) = \omega_p^2\omega_0/(\omega(\omega^2 + \omega_0^2) \quad (4)$$

ω_p and ω_0 are the frequencies of the plasma oscillation of free electron ($\omega_p = 1.38 \times 10^{16}$ s^{-1} for silver[40]) and of inelastic collisions of free electron within the metal, respectively.

When the particle size decreases, the rate of scattering from the particles surfaces, ω_s, greatly exceeds ω_0,[40] and the size effect is taken into account by replacing ω_0 by the surface scattering rate ω_s. A theoretical expression of ω_s is given by

$$\omega_s = \nu_f/R$$

where R is the particle's radius and ν_f the Fermi velocity (1.4×10^6 m s^{-1} for silver[38]). This corresponds to the limitation of the mean free path as the particle size decreases. To calculate the interband contribution ($\epsilon_{1IB}(\omega)$ and $\epsilon_{2IB}(\omega)$), it is assumed that it is size-independent; $\epsilon_1(\omega)$ and $\epsilon_2(\omega)$ are calculated from the bulk value of $n(\omega)$ and $k(\omega)$ commonly found in the literature.

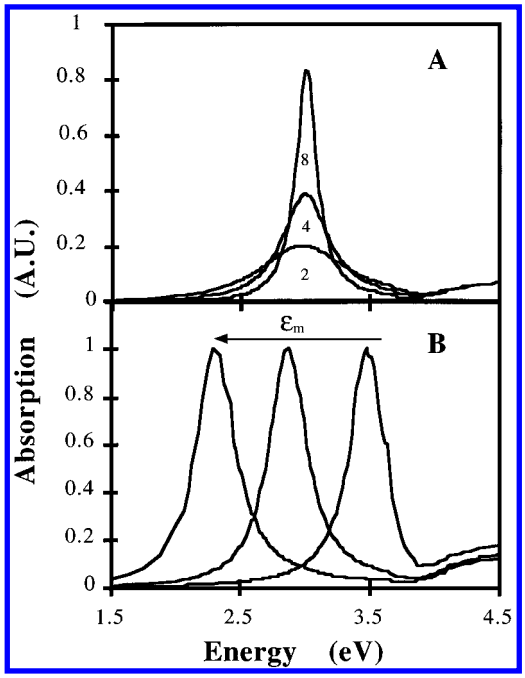

Figure 1. (A) Simulated absorption spectra of metallic silver particles differing by their size. Values of particles diameter in nm are indicated. (B) Simulated absorption spectra of 4-nm silver particles surrounded by a continuous media differing by the dielectric constant. Each spectrum is normalized at the maximum of the plasmon peak. From left to right, the dielectric constant of the media increases continuously.

TABLE 1: Theoretical Variation of the Bandwidth and the Peak Position with the Dielectric Constant of the Surrounding Media

	ϵ_m		
	1	3	6
fwhm (eV)	0.33	0.34	0.37
peak position (eV)	3.46	2.87	2.29

The absorption spectra of colloidal silver particles differing by their size are simulated by using eqs 3 and 4 with ω_s instead of ω_0. The relative permittivity of the surrounding medium, ϵ_m, is taken in eq 2 as that of hydrocarbon (Figure 1A). For large silver particles the plasmon peak is narrow and centered at 400 nm. The decrease in the particle size induces a decrease in the plasmon band intensity and an increase in the bandwidth.

Equation 1 clearly shows that the absorption spectrum of metal nanoparticles markedly depends on the dielectric constant of the surrounding media, ϵ_m. The simulated absorption spectrum of an isolated 4-nm silver nanosized particle shifts toward low energy with an increase in the bandwidth (Figure 1B and Table 1). This model is imperfect, as the matrix effect and the polydispersity are not taken into account even for isolated particles. However this model gives a qualitative account of the variation of the optical properties with the size or the surrounding medium. The former equations only hold

if the clusters do not interact. The absorption of a single spherical cluster is described as due to a dipole induced by the external electric field. If other clusters are nearby, the total electric field results from superposition of the external incident field and the dipole fields of all other clusters. Electromagnetic coupling of clusters is effective for cluster−cluster distances smaller than 5 times the cluster radius and may lead to complicated extinction spectra depending on size and shape of the formed cluster aggregate by a splitting of single cluster resonance.[41] Attempts have been made by using the generalized Mie theory to model the extinction spectra of organized monolayers of clusters.[47] However this calculation is limited to simple arrangement of 100 or fewer aggregates of large size (10−40 nm in diameter). The main effect is the splitting of the plasmon band resulting from the anisotropy of the monolayers. From our knowledge, for nanomaterials, the particle−particle electromagnetic coupling has not been calculated when the particles are arranged either in monolayers organized in a hexagonal network or in 3D superlattices in a face-centered cubic structure. To a first approximation, we could expect to find similar behavior with particles and clusters. Hence we could expect a shift in the plasmon peak to lower energy when the dielectric constant of the matrix environment increases.

IV. Syntheses of Silver Nanoparticles

Syntheses of silver nanosized particles in reverse micelles and control of the size distribution have been described previously.[23,24] Colloidal silver particles are prepared by mixing two AOT reverse micellar solutions having the same water content (i.e., molar ratio $W = [H_2O]/[AOT] = 40$). The first one is made with 30% Ag(AOT) and 70% Na(AOT), and the second one with N_2H_4, with 100% Na(AOT). The overall concentration of hydrazine is 7×10^{-2} M. The average diameter of the particles is 3.4 nm with 43% as size distribution. Dodecanethiol is added to the micellar solution (1 μL/cm^3), and a selective reaction with the silver atoms at the interface of the particles takes place. Ethanol addition to the micellar solution induces flocculation of the dodecanethiol-coated silver particles. The precipitate is then redispersed in hexane. This process with the different washing step prevents also the presence of excess ligand in the solution

To reduce the size distribution, a size-selected precipitation process is used.[24] A progressive addition of pyridine to hexane solution containing the silver-coated particles is performed. At a given volume of added pyridine (roughly 50%), the solution becomes cloudy and a precipitate appears, indicating agglomeration of the largest particles. The solution is centrifugated and an agglomerated fraction rich in large particles is collected, leaving the smallest particles in the supernatant. The precipitate, redispersed in hexane, forms a homogeneous clear solution. By repeating several times the same procedure on the first fraction and on the supernatant, the size distribution of silver particles of size 4.5, 5.2, and 6.1 nm reaches a value of roughly 13%.

V. Results and Discussion

1. Optical Properties of Individual Silver Nanoparticles in Hexane Solution. In our previous paper,[24] we showed that addition of dodecanethiol to silver nanoparticles made in reverse micelles induces a drastic decrease in the extinction coefficient, a shift toward the low energy, and an increase in the bandwidth of the plasmon peak, whereas no changes in the UV absorption spectrum are observed below 300 nm. Such behavior is attributed to a change in the free electron density resulting on the chemisorption of the sulfur headgroup to the metal surface. Similar behavior has been recently observed on gold particles.[40]

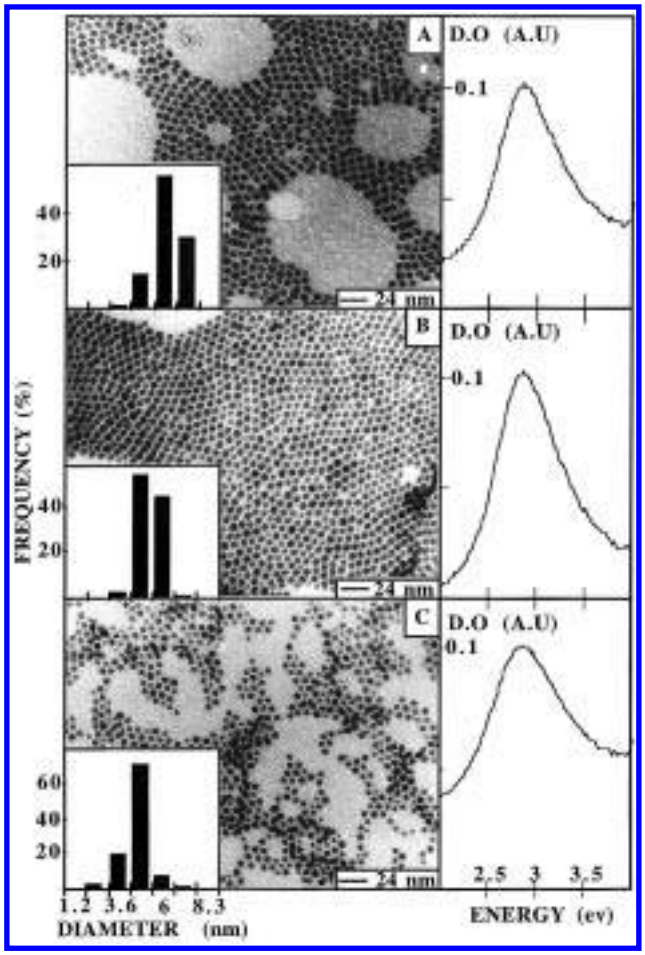

Figure 2. TEM micrograph, histograms, and UV−vis spectra of free silver-coated particles dispersed in hexane (A, 4.5 nm; B, 5.2 nm; C, 6.1 nm).

The absorption spectra of coated particles differing by their size are given in Figure 2. A negligible shift toward large energy is observed. However, as predicted, the plasmon peak bandwidth increases as the particle size decreases. The experimental bandwidths, determined from Figure 2, are always larger than that predicted from the Mie's model (Figure 1A). This could be due to the nature of the interaction of the surrounding medium with the surface of the particles as proposed by Charlé et al.[36]

2. Particles Organized in 2D and 3D Superlattices. The optical spectrum of the nanosize particles coated on graphite support is recorded by reflectivity mode and is compared with the spectrum corresponding to free particles in hexane. The optical spectra are normalized to unity.

A drop of a dilute solution of 4.5-nm-coated particles in hexane ($[(Ag)_n] = 2 \times 10^{-5}$ M) is deposited on a graphite surface. Figure 3A shows a large area of close packed nanoparticles organized in a hexagonal network. On a long-distance scale, large holes are observed (Figure 3B). This can be attributed to the bad wetting of hexane on graphite, which could induce hole nuclei. By complete evaporation of the solution, most of the particles are localized at the periphery of the holes; this favor a high organization of the particles. Recently, similar rings were observed with silver-coated particles in hexane deposited on a carbon surface.[42]

When the particles are organized in a 2D superlattice (Figure 3), the plasmon peak is shifted toward an energy lower than

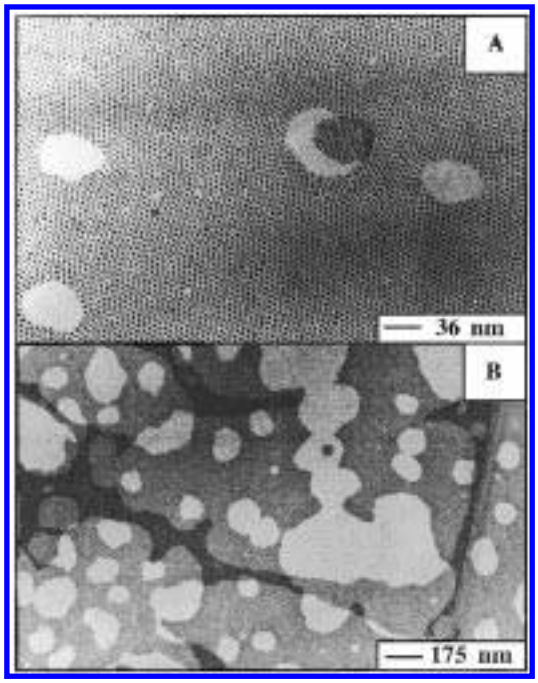

Figure 3. TEM micrograph of 4.5-nm silver particles deposited on graphite at rather small (A) and large distances (B).

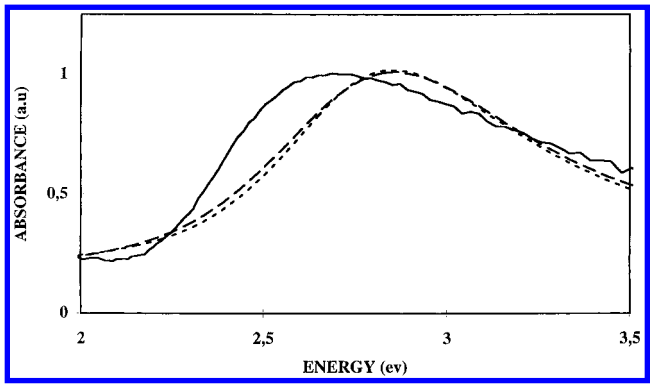

Figure 4. Absorption spectra of free 4.5-nm silver nanoparticles dispersed in hexane before (- - -) leaving a drop on the support, after washing the support with hexane (···), and deposition on the support forming a 2D superlattices (—) ($[(Ag)_n] = 2 \times 10^{-5}$ M).

that obtained in solution (Figure 4). The coverage support is washed with hexane and the nanoparticles are redispersed in the solvent. The absorption spectrum of the latter solution is similar to that used to cover the support (free particles in hexane). This clearly indicates that the shift in the absorption spectrum of nanosize silver particles is due to their self-organization on the support. The bandwidth of the plasmon peak (1.3 eV) obtained after deposition is larger than that in solution (0.9 eV). This can be attributed to a change in the dielectric constant of the composite medium. Taking into account the variation of the simulated plasmon peak (Figure 1B) with the dielectric constant, it is concluded that the shift toward lower energy observed in Figure 4 is due to an increase in the dielectric constant of the composite medium of the particles, which is the superposition of several factors[43] such as the spherical particles, the support, particle−particle interactions, and the air.

Similar behavior is observed for a diluted solution made of 5.2-nm and 6.1-nm nanosize particles.

By increasing the concentration of 4.5-nm nanoparticles in hexane solution ($[(Ag)_n] = 4 \times 10^{-3}$ M), the TEM pattern (Figure 5) shows large aggregates surrounded by smaller ones

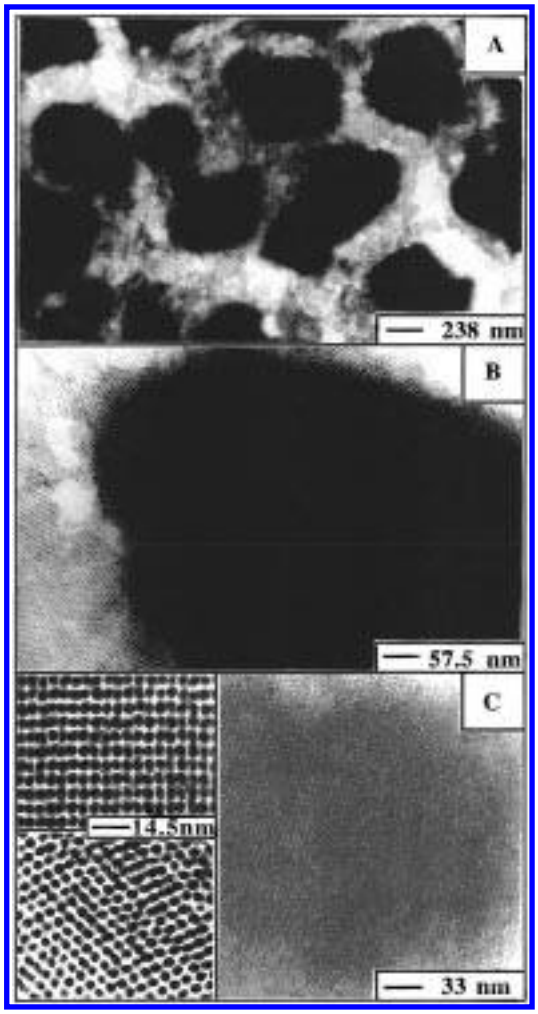

Figure 5. TEM micrographs obtained from a concentrated solution of 4.5 nm ($[(Ag)_n] = 4 \times 10^{-3}$ M) at low magnification (A), at higher magnification (B), and of an isolated aggregate (C). Insets show high resolution of different parts of the aggregate present in C.

and by monolayers. These aggregates are rather well faceted. High magnification of these aggregates (Figure 5C) confirms than they are made of nanoparticles. High resolution shows a 4-fold symmetry and hexagonal network (insets Figure 5C). This indicates formation of a polycrystalline phase. When the aggregates are small enough, monocrystals are obtained. The presence of 4-fold symmetry clearly indicates formation of a fcc structure. Such packing of silver nanoparticles has been demonstrated in our previous paper.[24] Similar self-assemblies of silver and gold nanoparticles have been obtained by using different experimental modes.[28−32] Simulations of gold clusters coated by dodecanethiol differing in numbers of atoms predict face-centered cubic (fcc) lattices with morphologies of a truncated octahedral motif.[44]

In some parts of the TEM grid shown in Figure 5, the aggregates are too large to be investigated by TEM.

By scanning electron microscopy, aggregates differing by their size and shape are observed (Figure 6). They are well-faceted, as observed for the smaller aggregate by TEM (Figure 5). We choose to investigate the aggregate given in Figure 6A. Enhancement of one face of the aggregate shows well-defined defects in the crystal phase (Figure 7A). The 60° tilt of aggregate shown in Figure 6A confirms a 3D structure (Figure 7B). This permits us to estimate the size of the aggregate, which is 200 μm high and 100 μm long. Figure 7B shows the presence of smaller aggregates surrounding the larger one. Furthermore,

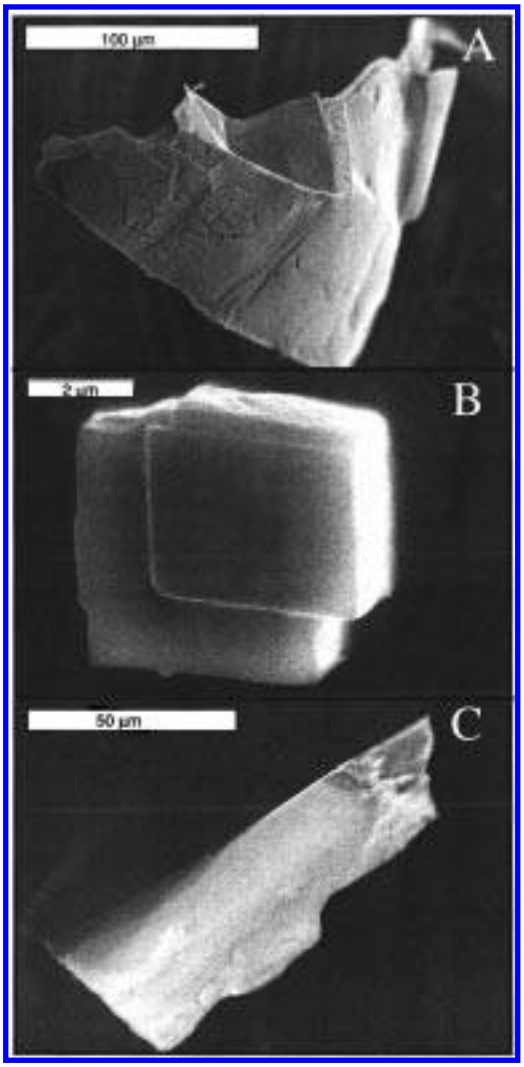

Figure 6. Difference in shape of aggregates determined by scanning electron microscopy on a concentrated solution of 4.5-nm silver particles ($[(Ag)_n] = 4 \times 10^{-3}$ M).

layers at the bottom of the aggregate are observed. To make sure that these aggregates are made of silver nanoparticles, EDX analyses were performed on the top of the aggregate and on the bottom (in the layers region). The analysis is made on a 0.786-μm^3 volume. The top of the aggregate (Figure 8A) consists of silver, carbon, and sulfur atoms. This is fully consistent with a crystal made of silver nanosized particles coated by dodecanethiol. Analysis of the layers observed on the surrounding of the aggregate reveals mainly the presence of carbon atoms due to cleaved graphite and traces of silver atoms. This confirms the presence of mono- and multilayers of silver nanosized particles observed by TEM.

The UV−visible spectrum (Figure 9) of the aggregates described above shows a 0.25-eV shift toward lower energy of the plasmon peak with a slight decrease in the bandwidth (0.8 eV) compared to that observed in solution (0.9 eV). As observed above with the monolayer, by washing the support, the particles are redispersed in hexane and the absorption spectrum remains similar to that of the colloidal solution used to make the self-assemblies.

For isolated particles, the increase in the dielectric constant induces a shift to lower energy and an increase in the bandwidth of the plasmon peak (Figure 1B). For particles organized in a fcc structure, each silver nanoparticle is surrounded by 12 other particles, whereas in a monolayer it has six neighbors. So in

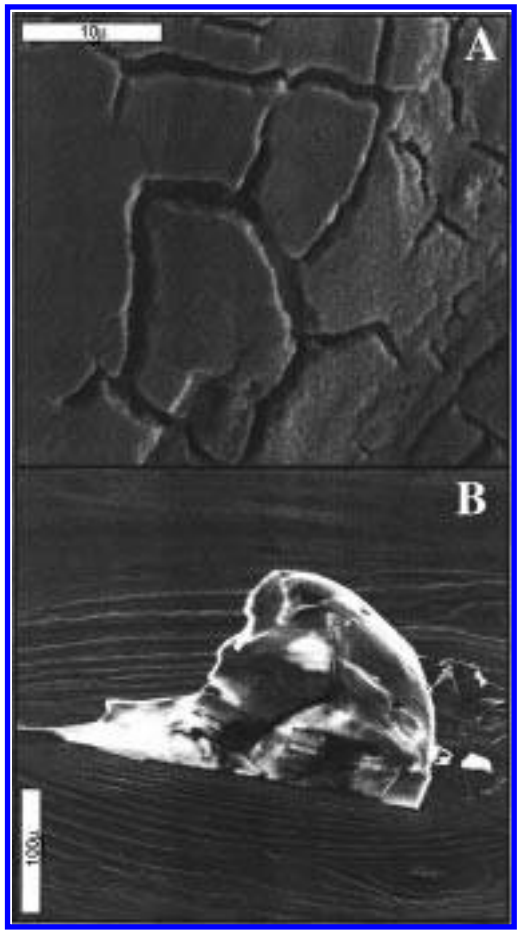

Figure 7. Scanning electron microscopy of the largest aggregates: (A) high magnification of the aggregate shown in Figure 6A; (B) tilt at 60° of the aggregate shown in Figure 6A.

3D superlattices, the dielectric constant must take into account the composite environment resulting from the external field, the dipole fields of all the other particles, and the contribution due to the support. There is no model actually which could evaluate quantitatively this effect, but all these effects must induce an increase in the total dielectric constant, which, as for isolated particles, induces a shift toward the low energy of the plasmon peak. This is confirmed when Figures 4 and 9 are compared: The shift of the plasmon peak of particles arranged in 2D and 3D superlattices compared with the spectrum corresponding to free coated particles in hexane is 0.12 and 0.25 eV, respectively. Hence, the increase in the total dielectric constant induces an increase in the plasmon peak bandwidth. This is not observed in Figure 9. The bandwidth is 0.8 eV, whereas for particles organized in 2D (Figure 4) it is 1.3 eV. The value obtained for a 3D superlattice (0.8 eV) is close to that observed for free nanoparticles in hexane (0.9 eV).

To confirm such behavior, we use 5.2-nm nanosized particles dispersed in hexane, ($[(Ag)_n] = 2.5 \times 10^{-3}$ M). Figure 10A shows the TEM pattern obtained by addition of one drop of the solution on the graphite support. Appearances of hole, mono-, and multilayers are observed. As expected from the previous data, the UV−visible absorption spectrum is shifted toward low energy (0.27 eV) compared to the absorption of particles dispersed in solution. The bandwidth of the plasmon peak (1.0 eV) is larger than that observed in solution (0.8 eV). As shown in Figure 10B, by adding three drops instead of one to the support, we obtain total coverage of the support. The increase in the TEM contrast indicates formation in some regions of 3D lattices. The absorption spectrum shows a large red shift of

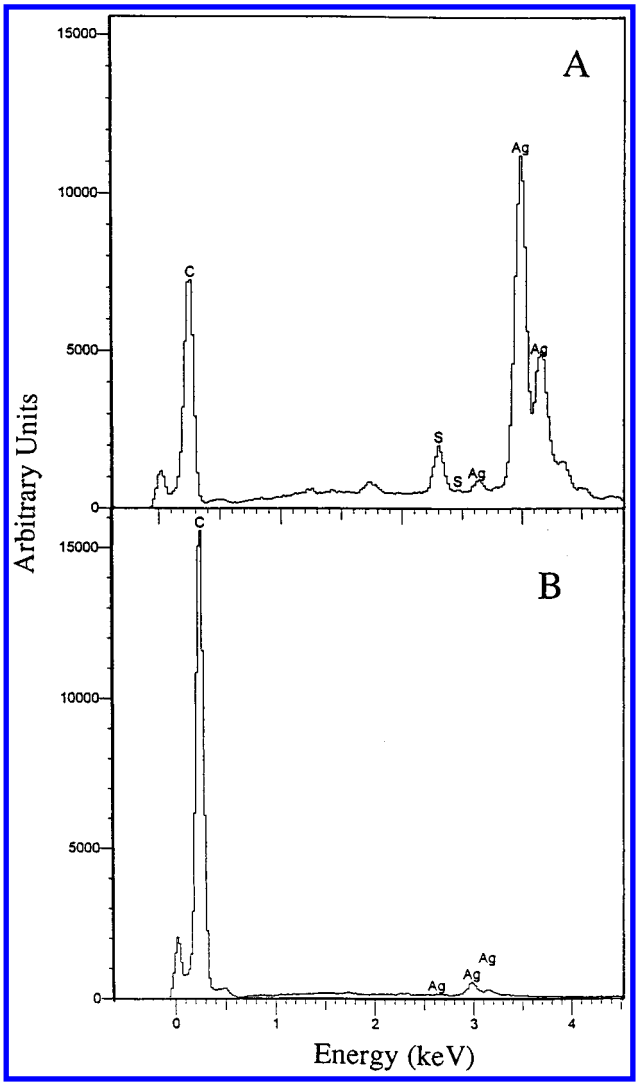

Figure 8. EDX analysis of the aggregate shown on Figure 7B: Analysis on the top (A) and on the surroundings (B) of the aggregate.

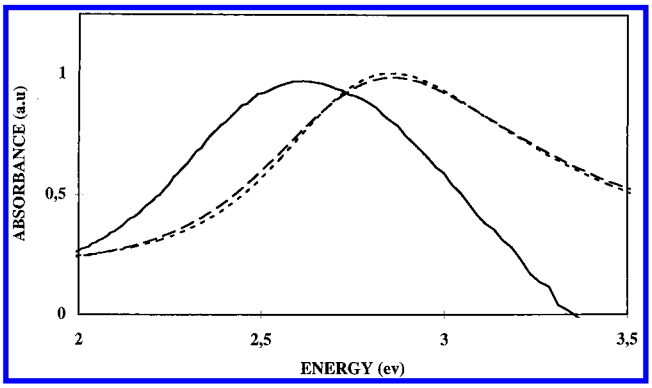

Figure 9. Absorption spectra of free 4.5-nm silver nanoparticles dispersed in hexane before (- - -) leaving a drop on the support, after washing the support with hexane (···), and deposition on the support forming a 3D superlattices (—) ($[(Ag)_n] = 4 \times 10^{-3}$ M).

the plasmon peak compared to the solution (0.47 eV) and to the absorption obtained from the pattern given in Figure 10A (0.27 eV). Furthermore, the bandwidth of the plasmon peak decreases (0.70 eV) in comparison with that obtained with the monolayer (1.0 eV) and is smaller than that obtained with free coated particles in hexane (0.80 eV). These data confirm the effect of the medium dielectric constant of the particle when organized in 2D and 3D and show a decrease in the bandwidth

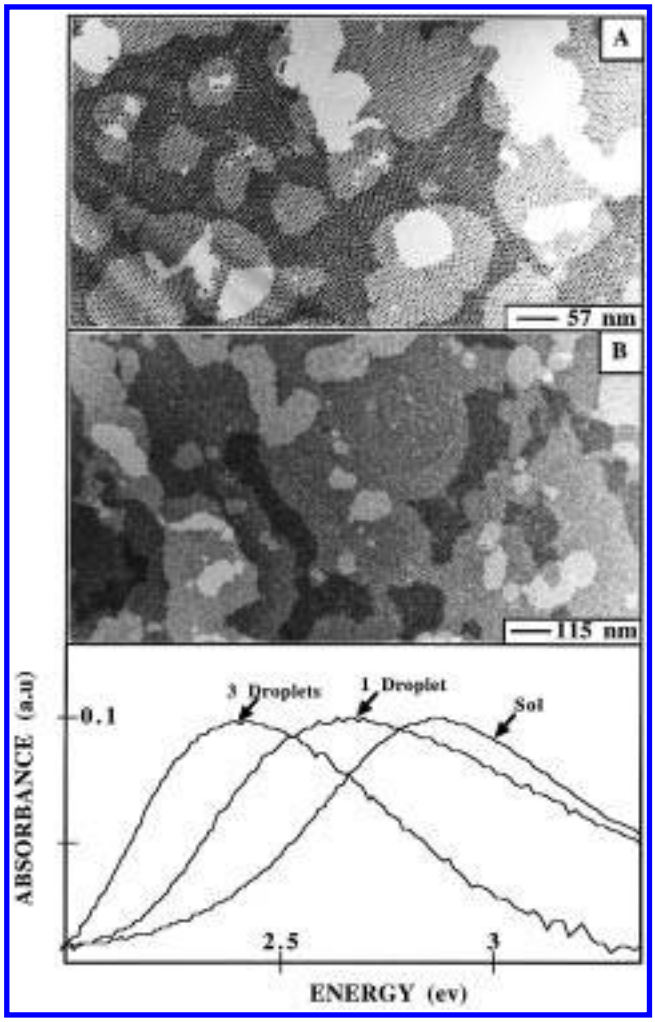

Figure 10. Effect on the number of droplets deposited on the monolayers on the extent of monolayers for 5.2-nm silver particles: (A) 1 droplet, (B) 3 droplets; (C) absorption spectra of the 4.5-nm silver nanoparticles dispersed in hexane before (1) and after (3) deposition and deduced from reflectivity when the particles are deposited on cleaved graphite ($[(Ag)_n] = 2.5 \times 10^{-3}$ M).

plasmon peak, which could be due to an increase in the mean free path conduction electrons of silver particles through a barrier of 2 nm. This is rather surprising, because the average distance between silver nanoparticles is 2 nm and we would not expect a tunneling electron effect through such a large barrier. However, a recent paper published by Ung et al.[45] claims that a 1−2 nm distance between two metal surfaces is enough for tunneling of electrons across the double layers. Because of the fact that we keep the same absorption spectrum and TEM pattern after washing the support, fusion between particles during the coverage can be excluded. No predictions have been given in the literature on the variation of the electromagnetic coupling of the particles when they are organized in 2D with a hexagonal network and 3D superlattices with a fcc structure. This does not permit us to definitively conclude on a collective effect, because of the transport of the conduction electrons through the barrier due to the coating. Recently similar data, which do not totally agree with those described in the present paper, indicate a decrease in the bandwidth of the plasmon peak: Heath et al.[31] showed, by using Langmuir−Blodgett technique, the formation of self-assemblies of silver and gold particles organized in monolayers forming a hexagonal network and densely packed but unorganized 3D arrangements. These self-assemblies were transferred on a carbon grid to get

TABLE 2: Experimental Variation of the Bandwidth and the Peak Position for Particles in Solution or Organized on Graphite in 2D or 3D

	sample A (4.5 nm)		sample B (5.2 nm)	
physical state	peak position (eV)	fwhm (eV)	peak position (eV)	fwhm (eV)
sol	2.85	0.9	2.88	0.8
2D	2.73	1.3	2.61	1
3D	2.6	0.8	2.41	0.7

a TEM pattern and on a glass for the optical experiments. With silver and gold particles coated with dodecanethiol they observed a red shift and a broadening of the plasmon peak. With gold particles coated with the C_9 ligand a sharpening of the plasmon peak is observed, whereas it was not with the C_{12} derivative. They attributed this to the fact that interparticle separation distance has to be sufficiently small to observe an appreciable delocalization of charges. This is in disagreement with the data presented in this paper where the sharpening of the plasmon peak appears when a 3D superlattice is obtained. Furthermore Heath et al. found no differences in the optical spectra with varying the film thickness. This is not the case in the present paper, in which a shift to lower energy and a decrease in the bandwidth of the plasmon peak is observed. These differences in the data could be attributed to the fact that in the present paper the optical experiments were performed on the same support as that used to observe the self-organization, whereas in the Heath et al.[31] paper the supports differed. No evidence is given for the fact that the self-organization remains the same by changing the support. This is supported by preliminary data obtained in our laboratory,[46] from which the self-organization of silver sulfide nanoparticles markedly differ with the support. Even with these differences in the data the fact that the bandwidth of the plasmon peak decreases and its maximum is red-shifted to lower energy indicate that a new phenomenon takes place when the particles are arranged in a fcc 3D superlattice. This arrangement is not present in the Heath experiment for similar particles coated with the same dodecanthiol. This could be attributed to a tunneling effect across the coating of the particles. Currently we are doing electrical conductance from which we hope to confirm the interpretation of our results.

V. Conclusion

By deposition of nanosized particles on a graphite support, self-organizations in 2D and 3D superlattices are observed. Very large aggregates can be produced.

The optical properties of nanoparticles deposited on cleaved graphite behave differently with the self-organization (see Table 2).

(i) When the particles are organized in a 2D hexagonal network, the plasmon peak is shifted toward low energy and an increase in the bandwidth is observed. This is attributed to an increase in the dielectric constant of the nanoparticle surroundings.

(ii) In a 3D superlattice the self-organization induces an increase in the medium dielectric constant, which provokes a larger shift toward low energy compared to the 2D superlattice. To this behavior is added an opposite effect, due to a change in the mean free path of conduction electrons, which induces a decrease in the bandwidth. Hence, tunneling of electrons across the coating of particles could take place.

Acknowledgment. The authors wish to thank Professors K. Charle and B. Ninham for fruitful discussions and O. Araspin for his technical assistance with the SEM experiment and EDX analysis.

References and Notes

(1) Special issue: Nanostructured Materials, *Chem. Mater.* **1996**, *8* (5).
(2) Special issue: *Science* **1996**, *271*, 920−941.
(3) Heath, J. R. *Science* **1995**, *270*, 1315.
(4) Mie, G. *Ann. Phys.* **1908**, *25*, 377.
(5) Wokaun, A.; Gordon, J. P.; Liao, P. F. *Phys. Rev. Lett.* **1982**, *48*, 957.
(6) Doremus, R. H.; Pratima R. *J. Mater. Res.* **1996**, *11*, 2834.
(7) Kreibig, U.; Fragstein C. v. *Z. Phys.* **1962**, *224*, 307.
(8) Meier, M.; Wokaun, A. *Opt. Lett.* **1983**, *8*, 581.
(9) Lam, C. C.; Leung, P. T.; Young, K. *J. Opt. Soc. Am. B* **1992**, *9*, 1585.
(10) Genzel, L.; Martin, T. P.; Kreibig, U. *Z. Phys. B.* **1975**, *21*, 339.
(11) Pileni, M. P. *J. Phys. Chem.* **1993**, *97*, 6961.
(12) Pileni, M. P. *Langmuir* **1997**,13, 3266.
(13) Fendler, J.; Meldrum, F. C. *Adv. Mater.* **1995**, *7*, 607.
(14) Solecka-Cermakova, K.; Vlckova, B. *J. Phys. Chem.* **1996**, *100*, 4954.
(15) Badia, A.; Gao. W.; Singh, S.; Demers, L.; Cuccia, L.; Reven, L. *Langmuir* **1996**, *12*, 1262.
(16) Brust, M.; Bethell, D.; Schiffrin, D. J.; Kiely, C. J. *Adv. Mater.* **1995**, *7*, 795.
(17) Spatz, J. P.; Roescher, A.; Moller, M. *Adv. Mater.* **1996**, *8*, 337.
(18) Kimizuka, N.; Kunitake, T. *Adv. Mater.* **1996**, *8*, 89.
(19) Tse, A. S.; Wu, Z.; Asher, S. A. *Macromolecules* **1995**, *28*, 6533.
(20) Asher, S. A.; Holtz, J.; Liu, L.; Wu, Z. *J. Am. Chem. Soc.* **1994**, *116*, 4997.
(21) Chang, S. Y.; Liu, L.; Asher, S. A. *J. Am. Chem. Soc.* **1994**, *116*, 6739.
(22) Giersig, M.; Mulvaney, P. *Langmuir* **1993**, *9*, 3408.
(23) Petit, C.; Lixon, P.; Pileni, M. P. *J. Phys. Chem.* **1993**, *97*, 12974.
(24) Taleb, A.; Petit, C.; Pileni, M. P. *Chem. Mater.* **1997**, *9*, 950.
(25) Motte, L.; Billoudet, F.; Pileni, M. P. *J. Phys. Chem.* **1995**, *99*, 16425.
(26) Motte, L.; Billoudet, F.; Lacaze E.; Pileni M. P. *Adv. Mater.* **1996**, *8*, 1018.
(27) Motte, L.; Billoudet, F.; Lacaze, E.; Douin, J.; Pileni, M. P. *J. Phys. Chem.* **1997**, *101*, 138.
(28) Whetten, R. L.; Khoury, J. T.; Alvarez, M. M.; Murthy, S.; Vezmar, I.; Wang, Z. L.; Cleveland, C. C.; Luedtke, W. D..; Landman, U. *Adv. Mater.* **1996**, *8*, 429.
(29) Brust, M.; Bethell, D.; Schiffrin, D. J.; Kiely, C. J. *Adv. Mater.* **1995**, *7*, 9071.
(30) Harfenist, S. A.; Wang, Z. L.; Alvarez, M. M.; Vezmar, I.; Whetten, R. L. *J. Phys. Chem.* **1996**, *100*, 13904.
(31) Heath, J. R.; Khobler, C. M.; Leff, D. *J. Phys. Chem. B* **1997**, *101*, 189.
(32) Harfenist, S. A.; Wang, Z. L.; Whetten, R. L.; Vezmar, I.; Alvarez, M. M.; *Adv. Mater.* **1997**, *9*, 817.
(33) Petit, C.; Lixon, P.; Pileni, M. P. *Langmuir* **1991**, *7*, 2026.
(34) *Absorption and Scattering of Light by Small Particles*; Bohren, C. F., Huffman, D. R., Eds.; Wiley: New York, 1983.
(35) Mochizuki, S.; Ruppin, R. *J. Phys.: Condens. Matter* **1993**, *5*, 135.
(36) Charlé, K. P.; Schulze, W. *Ber. Bunsen-Ges. Phys. Chem.* **1984**, *88*, 350.
(37) Greighton, J. A.; Eaton, D. G. *J. Chem. Soc., Faraday Trans. 2* **1991**, *87*, 3881.
(38) Hövel, H.; Fritz, S.; Hilger, A.; Kreibig, U.; Vollmer, M. *Phys. Rev. B* **1993**, *48*, 18178.
(39) Persson, B. N. J.; *Surf. Sci.* **1993**, *281*, 153.
(40) Alvarez, M. A.; Khoury, J. T.; Shaaf, T. G.; Shafigullin, M. N.;Vezmar, I.; Whetten, R. L. *J. Phys. Chem. B* **1997**, 101, 3706.
(41) Quinten, M.; Kreibig, U.; *Appl. Opt.* **1993**, *32*, 6173.
(42) Ohara, P. C.; Heath, J. R.; Gelbart, W. M.; *Angew. Chem. Int. Ed. Eng.* **1997**, *36*, 1077.
(43) Ninham, B. W.; Sammut, R. A. *J. Theor. Biol.* **1976**, *56*, 125.
(44) Luedthe, W. D.; Landman, U. *J. Phys. Chem.* **1996**, *32*, 13323.
(45) Ung, T.; Giersig, M.; Dunstan, D.; Mulvaney, P. *Langmuir* **1997**, *13*, 1773.
(46) Motte, L.; Lacaze, D.; Pileni, M. P. In preparation.
(47) *Optical Properties of Metal Cluster*, Springer Series in Materials Science, Vol 25; Kreibig, U., Vollmer, M., Eds.; Springer-Verlag: Berlin, 1995.